Chemical Engineering & Technology

Chemical & Engineering Technology

RESEARCH ARTICLE OPEN ACCESS

Effect of Pyrolysis Temperature on Phosphorus Release From Fish Scale Biochar in Wheat Crop

Guilherme S. Vitor[1] | Andressa M. Paiva[2] | Túlio P. Boaventura[2] | Leônidas C. Azevedo Melo[3] | Juliano E. Oliveira[4]

[1]Department of Environmental Engineering, Universidade Federal de Lavras, Lavras, Minas Gerais, Brazil | [2]Graduate Program in Agrochemical, Universidade Federal de Lavras, Lavras, Minas Gerais, Brazil | [3]Department of Soil Science, Universidade Federal de Lavras, Lavras, Minas Gerais, Brazil | [4]Department of Chemistry and Materials Engineering, Universidade Federal de Lavras, Lavras, Minas Gerais, Brazil

Correspondence: Juliano E. Oliveira (juliano.oliveira@ufla.br)

Received: 12 June 2025 | **Revised:** 20 January 2026 | **Accepted:** 30 January 2026

Keywords: circularity | fish farming waste | *Oreochromis niloticus* | slow-release fertilizer | sustainable agriculture

ABSTRACT

The conversion of agroindustrial waste into functional materials supports sustainable process engineering by enabling controlled phosphorus (P) release to improve nutrient use efficiency and reduce environmental impacts. This study assesses biochar from fish scales as a sustainable P source. Biochars produced at temperatures between 300°C and 600°C were characterized by yield, PZC, TGA, FTIR, SEM, elemental analysis, and total/available P by ICP-OES. Phosphorus release kinetics were fitted to mathematical models. Increased pyrolysis temperature enhanced available P. The Korsmeyer–Peppas model best described release, indicating diffusion-controlled slow release. Carbon content decreased with higher pyrolysis temperature. Wheat greenhouse trials confirmed fertilizer efficacy. Fish scale biochar is a promising sustainable phosphate source for process-oriented agricultural technologies.

1 | Introduction

Biochars obtained from fish scales are a form of carbon-rich material produced through the pyrolysis of fish scales at high temperatures in an oxygen-limited environment [1]. These biochars are characterized by their porous structure, high surface area, and significant mineral content, including calcium and phosphorus [2]. They offer unique properties for applications in soil enhancement, water filtration, and carbon sequestration due to their bioactive components and nutrient retention capabilities [3].

Unique properties of biochar make it a valuable tool in agriculture, enhancing soil fertility, nutrient retention, and crop yield while reducing environmental impact [4]. Engineered biochar can significantly enhance soil properties, including pH, nutrient availability, and microbial activity [5]. This leads to improved soil fertility and increased crop productivity. The porous structure of biochar helps retain water and nutrients, making them more available to plants. By stabilizing carbon in the soil, biochar contributes to long-term carbon sequestration, thus mitigating climate change. The stability of biochar in soil prevents the rapid release of carbon dioxide back into the atmosphere [6]. The application of biochar improves soil structure by increasing its aeration and reducing bulk density. This is particularly beneficial for compacted soils, enhancing root growth and plant health [7].

Despite its numerous benefits, the application of biochar as a soil fertilizer faces several challenges as low nutrient content. The utilization of phosphorus-rich agro-industrial residues for biochar production represents a promising approach for the development of organic phosphate fertilizers [8]. These

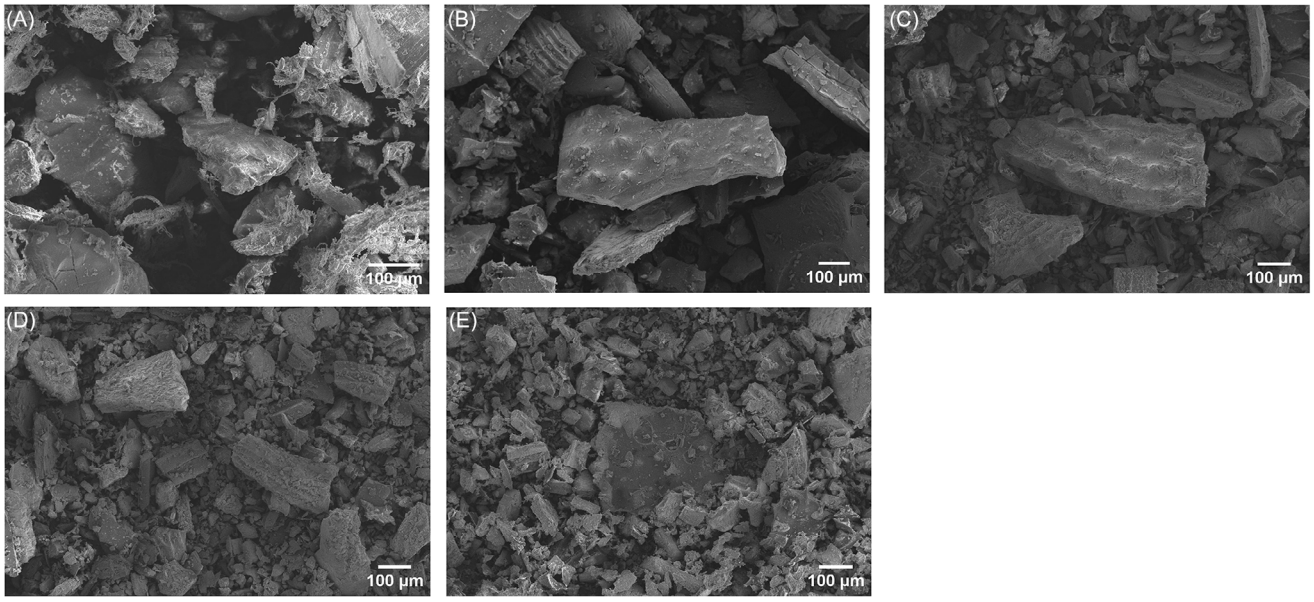

FIGURE 1 | SEM images in the figure for biochar from fish scale for different pyrolysis temperatures: (A) fish scale; (B) 300°C; (C) 400°C, (D) 500°C, and (E) 600°C.

innovative fertilizers possess significant potential to ensure a sustainable phosphorus supply for agriculture by adhering to the principles of a circular economy [9]. Specifically, the waste generated by the fish industry can be effectively recycled and repurposed as agricultural inputs, thereby closing the nutrient loop and enhancing resource efficiency [10].

The use of agro-industrial residues rich in phosphorus for the production of biochar is an excellent alternative for the production of organic phosphate fertilizers [11]. These new fertilizers have great potential to guarantee phosphorus supplies for agriculture through the concept of circular economy, as all waste generated by the fish industry can be returned as agricultural input [12].

Fish scale is a residue rich in calcium phosphate and therefore becomes an excellent candidate for the production of biochars for the slow release of phosphorus [13]. Phosphorus is critically important for wheat crops growth and development, influencing various physiological and biochemical processes that directly affect yield and quality. Proper management of phosphorus fertilization is crucial to maximize wheat productivity and ensure sustainable agricultural practices [14].

The main objective of the present study was to determine the effects of pyrolysis temperature on the structure, morphology, and phosphorus release parameters of fish scale biochars and their application in wheat cultivation in greenhouse experiments.

2 | Results and Discussion

2.1 | Scanning Electron Microscopy (SEM)

Figure 1 presents SEM micrographs of fish scale–derived biochar obtained at progressively higher pyrolysis temperatures. Across all samples (Figure 1A–E), the carbonized matrix exhibits irregular, angular fragments with sharp edges, indicating brittle fracture behavior. Particle dimensions predominantly span from approximately 76 to 218 µm, although occasional agglomerates exceed this range. As the pyrolysis temperature increases (notably in Figure 1E), a marked reduction in the mean particle size (76 µm) is evident, which can be attributed to the enhanced devolatilization rates and intensified carbonization kinetics at elevated temperatures. Contrary to many lignocellulosic biochars, these fish scale biochars lack well-developed pore networks, displaying predominantly nonporous surfaces. This limited porosity is consistent with the high inorganic fraction inherent to hydroxyapatite-rich fish scales, which inhibits pore formation during thermal decomposition. The plate-like morphology observed in lower temperature samples (Figure 1A,B) transitions toward finer, more fragmented debris at higher temperatures (Figure 1C–E), reflecting progressive matrix embrittlement. Overall, the SEM analysis confirms that although higher temperatures promote particle comminution through carbon matrix contraction and mineral crystallite growth, they do not induce significant pore development in fish scale biochars due to the dominant mineral phase. Additionally, with the gradual increase in pyrolysis temperature, it can be clearly observed that the structure was broken (Figure 1A–E), forming uniform structures, and the overall biochar scale structure also collapsed; the previously well-defined lamellae appeared disrupted, fragmented, and agglomerated to form an irregular loose morphology [15].

Figure 2 presents SEM micrographs alongside energy-dispersive x-ray spectroscopy (EDS) phosphorus maps (blue overlay) of fish scale–derived biochars produced at successive pyrolysis temperatures. In the unpyrolyzed control (A, A1), phosphorus appears localized in discrete, uneven patches corresponding to native hydroxyapatite domains. Upon thermal treatment at 300°C (B, B1), phosphorus mapping reveals a more uniform dispersion of P-bearing phases, suggesting initial breakdown of organic matrix and partial migration of phosphate minerals across the

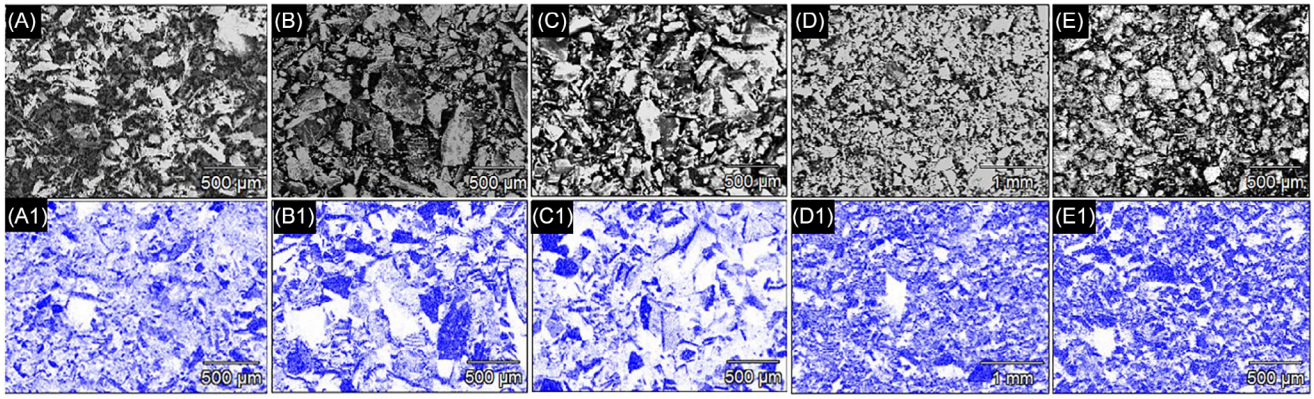

FIGURE 2 | SEM images with EDS phosphorus mapping of biochar from fish scale for different pyrolysis temperatures: (A and A1) fish scale, (B and B1) 300°C, (C and C1) 400°C, (D and D1) 500°C, and (E and E1) 600°C.

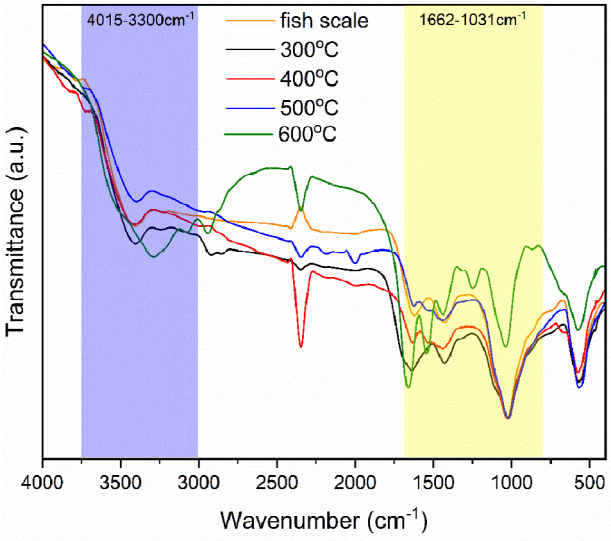

FIGURE 3 | Fourier-transform infrared spectra (FTIR) for biochar from fish scales for different pyrolysis temperatures.

char surface. At 400°C (C, C1), the blue signal intensifies and covers a greater fraction of the surface, indicating enhanced exposure and possibly recrystallization of phosphate species as volatile organics are expelled. By 500°C (D, D1), phosphorus mapping demonstrates continuous, interconnected domains of P-rich regions, reflecting coalescence of phosphate particles. In the highest temperature sample (E, E1), phosphorus remains widely distributed.

These EDS results imply that pyrolysis temperature critically governs both the accessibility and spatial distribution of phosphorus in fish scale biochars. Lower temperatures preserve mineral heterogeneity, while intermediate regimes (300–500°C) optimize P exposure through biochar matrix decomposition.

2.2 | Infrared Spectroscopy

Figure 3 illustrates the transformation of biochar surface functionalities as a function of pyrolysis temperature, elucidating the complex interplay between thermal decomposition and carbonaceous structural reorganization. Advanced Fourier-transform infrared (FTIR) spectroscopic analysis reveals a systematic decline in the abundance of reactive surface sites with increasing thermal treatment.

This phenomenon is primarily attributable to the rapid volatilization of labile organic compounds and the concomitant enhancement in the degree of carbonization. In the FTIR spectra, a broad absorption band spanning 3300–4015 cm^{-1} is observed, corresponding to the O–H stretching vibrations of alcoholic and phenolic hydroxyl groups. At elevated pyrolysis temperatures, this band exhibits increased width and intensity due to enhanced thermal activation, although such signals are negligible in the precursor fish scale material prior to thermal processing.

At a pyrolysis temperature of approximately 600°C, a distinct absorption peak emerges at 2943 cm^{-1}, indicative of C–H stretching vibrations within aliphatic alkyl chains. Concurrently, the spectral feature at 1662 cm^{-1} is assigned to the stretching of carbonyl (C═O) bonds, characteristic of carboxylic functionalities or conjugated ketonic structures. Additionally, a stretching vibration attributed to aliphatic C═C bonds is detected at 1543 cm^{-1}, reflecting the presence of unsaturated hydrocarbon segments within the evolving carbon matrix.

Thermal decomposition studies indicate that the cleavage of hydroxyl groups from aliphatic chains predominantly occurs between 120°C and 200°C. As pyrolysis progresses to approximately 400°C, extensive cracking of aliphatic fragments, such as methyl, methylene, and methoxyl groups, ensues, accompanied by the formation of new carbonyl and carboxyl functionalities. Notably, heteroaromatic and aromatic moieties exhibit considerable thermal stability at these intermediate temperatures. Beyond 600°C, aliphatic functionalities are effectively eradicated, as these groups are converted into more thermodynamically stable aromatic and graphitic structures. This transformation is evidenced by the attenuation of absorption peaks between 1540 and 1660 cm^{-1}, resulting in a biochar product with a higher fixed carbon content and diminished surface oxygenation.

The observed modifications in biochar surface chemistry driven by dehydroxylation, dealkylation, and aromatization reactions bear significant implications for its applications as soil fertilizer.

TABLE 1 | Effect of temperature of pyrolysis on pH_{pcz}, yield, and phosphorus content in fish scale biochar.

	pH_{pcz}	pH	Yield (%)	Ash content	Total P (g kg^{-1})	Available P (g kg^{-1})	Available P (%)
Fish scale	—	—	—	—	91.8 ± 5.6c	65.7 ± 1.6d	71.8 ± 5.4b
300°C	7.58b	6.75a	70.4a	49.68 ± 3.85a	138.8 ± 9.0b	95.3 ± 6.2c	68.7 ± 0.3b
400°C	7.91ab	7.57ab	55.5b	50.05 ± 1.39b	173.6 ± 12.8a	138.4 ± 4.1b	75.9 ± 3.0b
500°C	7.70b	7.90b	50.0c	36.64 ± 0.71c	183.9 ± 6.1a	141.3 ± 4.4ab	78.0 ± 3.1ab
600°C	8.83a	8.13b	50.0c	36.41 ± 0.51c	172.0 ± 2.1a	150.1 ± 4.6a	84.1 ± 5.2a

Note: Results followed by different letters indicate a significant difference ($p < 0.05$) by ANOVA followed by Tukey's test at 5%.

Understanding the temperature-dependent evolution of these functional groups is crucial for tailoring biochar properties to sustainable agriculture, thereby optimizing performance in targeted crops.

The interplay between reaction kinetics, mass transfer, and structural reconfiguration is pivotal in dictating the final composition and performance characteristics of biochar. Such insights are invaluable for the rational design of high-performance carbon-based materials in energy storage, environmental remediation, and catalysis, bridging the gap between fundamental science, materials engineering, and agriculture application.

2.3 | Phosphorus Content

Table 1 summarizes the influence of pyrolysis temperature on biochar yield, ash content, point of zero charge (PZC) (pH_{pzc}), and phosphorus speciation relative to the raw fish scale precursor. As the pyrolysis temperature rises from 300°C to 600°C, the mass yield of biochar declines markedly from approximately 70% at 300°C to 50% at 600°C reflecting progressive devolatilization and loss of organic fractions. Concomitantly, the pH_{pzc} shifts toward more alkaline values (from near neutral in the precursor to pH 8.8 in high-temperature biochars), owing to increased concentration of basic mineral oxides and carbonates formed during high-temperature carbonization.

The pH_{pzc} values of biochars obtained at different temperatures of pyrolysis were lower than biochar obtained by fish bone reported in previous studies [16]. In addition, the interaction between biochar surface charge (pH_{pzc}) and soil pH critically influences ions phosphate adsorption–desorption dynamics. The wheat-used soil displayed a native pH of 5.7, which lies below the PZC measured for all biochars ($pH_{pzc} \approx 7.6$ at 300°C, rising to ~8.3 at 600°C). Under these conditions, the biochar surfaces bear a net positive charge, favoring electrostatic attraction of negatively charged phosphate ions ($H_2PO_4^-$, HPO_4^{2-}).

The pH values are also shown in Table 1. It is noted that, with the increase in pyrolysis temperature, the pH of the biochars increased, going from 6.75 at 300°C to 8.13 at 600°C. The materials produced at higher temperatures showed greater basicity, which is associated with recent studies showing that biochars produced at higher temperatures tend to have higher pH values due to the loss of acidic functional groups and the higher concentration of alkaline minerals in their composition. This results from the ash, causing an increase in the basicity of the materials [17].

Fish scale biochar showed higher ash content at lower pyrolysis temperatures (300°C and 400°C), with a significant reduction at 500°C and 600°C, highlighting the effect of temperature on the volatilization of organic matter and the distribution of the mineral fraction. Behavior consistent with that reported for biochars from different biomasses [18].

Similar developments in phosphorus availability with increasing pyrolysis temperature were observed in biochars derived from animal bones, where thermal conversion stabilizes calcium phosphates and increases the exposure of phosphate surfaces of the material, resulting in greater P availability and fertilizer potential in the soil after pyrolysis [19].

Total phosphorus content (total P) in the biochar increases with temperature when expressed on a mass-normalized basis, rising from 139 g P kg^{-1} at 300°C to 172 g P kg^{-1} at 600°C. This enrichment results from removal of volatile C-rich matter and concentration of the inorganic hydroxyapatite phase. The fraction of phosphorus in readily soluble forms (available P) shows an increase with temperature. At 300°C, available P is moderately high 95 g P kg^{-1}), corresponding to 69% of total P, as early carbonization exposes labile phosphate sites. With further temperature increase to 400–500°C, available P reaches a maximum (150 g P kg^{-1}; 84% of total P) due to optimized breakdown of the organic matrix and increased surface reactivity.

In comparison to unpyrolyzed fish scale (total P 92 g P kg^{-1}; available P 66 g P kg^{-1}; 72% available), optimal pyrolysis at 600°C yields biochars that balance high total phosphorus concentration with enhanced available P fraction.

2.4 | Isothermal Analysis of Pyrolysis

The thermal degradation behavior of biochar and the effects of varying temperatures on its isothermal pyrolysis were systematically evaluated. Initially, the temporal mass loss profile of fish scale–derived biochar under different isothermal conditions was analyzed to determine the optimal pyrolysis residence time, with the corresponding data presented in Figure 4. As depicted, the fish scale underwent rapid devolatilization during the first 3000 s, after which the pyrolysis rate declined post-5600 s. Notably, only a 1% reduction in residual mass fraction was recorded between 5600 and 10 000 s. These findings suggest that the most intense decomposition occurs within the first 3000 s, and by 10 000 s, the residual mass fraction approximates the final stabilized weight fraction, designated as W_f.

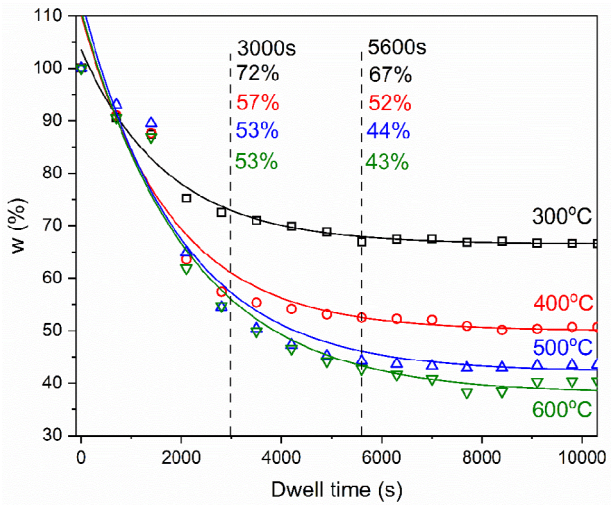

FIGURE 4 | The weight loss curve of the fish scale pyrolysis under different isothermal conditions.

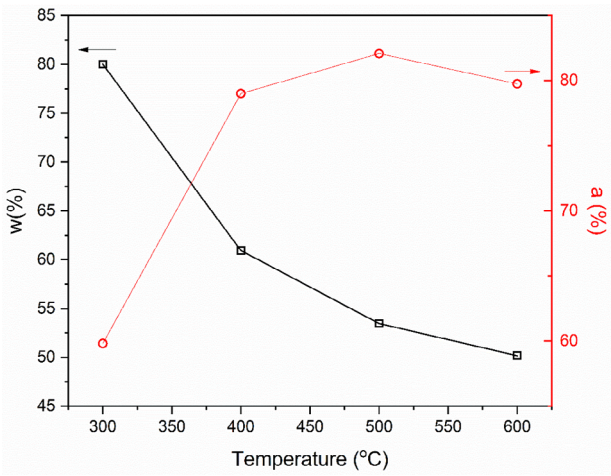

FIGURE 5 | Pyrolysis curves of fish scale under different isothermal conditions.

The temperature-dependent pyrolysis behavior of fish scale was subsequently examined (Figure 5). Initially, the sample underwent a drying phase at 80°C, followed by isothermal pyrolysis initiated at 300°C using a controlled heating rate of 30°C min^{-1}.

The evolution of mass loss was monitored under isothermal conditions spanning from 300°C to 600°C (Figure 5). As the temperature increased, the residual mass fraction exhibited a progressive decline. At the lower temperature regime (300–400°C), the fish scale primarily experienced thermal cracking and collagen depolymerization, characterized by the cleavage of structural bonds and the degradation of functional groups, which resulted in the liberation of a significant volume of volatile compounds and marked mass loss. In contrast, above 500°C, the reduction in weight loss rate was more gradual, a phenomenon likely attributable to the thermolytic decomposition of calcium phosphate and other mineral constituents inherent to the fish scale. Consistent with recent kinetic studies and pyrolysis analysis with animal biomass waste, the thermal decomposition behavior is highlighted as varying significantly with temperature and material composition. Devolatilization of organic matrices at lower temperatures results in rapid mass loss followed by slower transformations of mineral components at temperatures above 400°C [20]. The apparent plateau in biochar yield above 400°C can be explained by the transition between distinct thermal degradation stages during pyrolysis. At temperatures below approximately 400°C, the process is dominated by primary devolatilization of the organic matrix, resulting in rapid mass loss due to the release of moisture, proteins, lipids, and other volatile compounds. Above 400°C, the remaining solid phase consists predominantly of thermally stable carbonaceous and mineral components. In this high-temperature regime, further mass loss is mainly associated with secondary devolatilization and slow structural rearrangements, such as aromatization and condensation reactions, which have a limited impact on the overall mass of the solid residue. Consequently, although the total mass of the fish scales continues to decrease slightly with increasing temperature, the biochar yield stabilizes, leading to the observed plateau in Figure 5.

Furthermore, conversion rate analysis indicated that approximately 80% conversion was achieved at 600°C, suggesting that further increases in temperature yield marginal improvements in conversion efficiency. Consequently, from the standpoint of optimizing biochar synthesis, an isothermal pyrolysis temperature of around 600°C appears to be the most advantageous. This conversion rate presented in Figure 5 does not represent the biochar yield. In biomass pyrolysis for biochar production, conversion rate (a) and yield describe related but distinct concepts. The conversion rate (a) measures the fraction of biomass decomposed during pyrolysis, calculated from the change in mass relative to the initial and final solid masses under controlled conditions. It reflects the extent of thermal degradation or reaction progress. In contrast, the yield refers to the mass fraction of biochar obtained after pyrolysis. Yield depends on operating parameters like temperature and residence time and represents the distribution of final products rather than the kinetic degree of conversion.

2.5 | Phosphorus Release

Figure 6 illustrates the cumulative phosphorus release profiles obtained from fish scale biochars processed via pyrolysis at distinct temperatures. Samples pyrolyzed at 300°C and 400°C (depicted in Figure 6A) and those processed at 500°C and 600°C (Figure 6B) exhibit differences in release kinetics behavior.

Notably, the phosphorus elution rate from the unpyrolyzed fish scale significantly exceeds that of the pyrolyzed biochars under all temperature conditions. Although phosphorus is rapidly liberated from the fish scale substrate, complete nutrient discharge is not achieved even after 240 h. This incomplete release is attributable to the intrinsic composite structure of fish scales, comprising a biogenic microstructure of calcium phosphate and collagen, and the limited porosity observed in the resulting biochars as confirmed by SEM (Figure 1). Pyrolysis substantially reduces phosphorus release, with more pronounced suppression at higher processing temperatures. Specifically, phosphorus release decreases from 56% in the unpyrolyzed biomass to 47% at 300°C, 43% at 400°C, 44% at 500°C, and 46% at 600°C over a 72-h interval. These results agree with the study by Liang et al. [21],

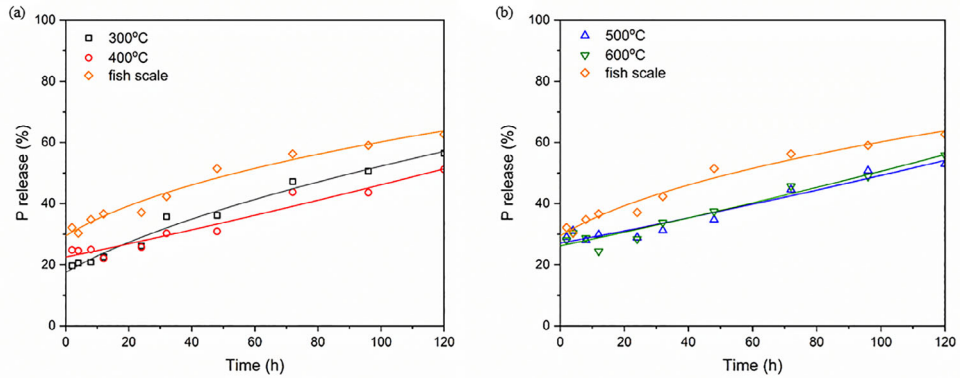

FIGURE 6 | Kineticsof phosphorus release into water from fish scales and biochars pyrolyzed at 300 and 400°C (a) and 500 and 600°C (b).

which mentions a slower and lower release in biochar derived from manure compared to manure. Similar to biochar of fish scale studied in this work, phosphorus release in manure biochar reported by literature was rapid in the first 48 h (burst release) but remained stable without reaching equilibrium even after 240 h of testing. Similar to scale biochar, phosphorus release in manure biochar was rapid in the first 48 h but remained stable without reaching equilibrium even after 240 h of testing. The authors attribute this rapid initial release to the dissolution of low-crystallinity or amorphous phosphate groups [21]. In fish scales, phosphorus release is mainly driven by matrix swelling, collagen relaxation, and nutrient diffusion from the swollen biocomposite. Conversely, phosphorus elution from biochars is predominantly governed by Fickian diffusion, necessitating the detachment of phosphorus species from the carbonaceous matrix. Additionally, higher pyrolysis temperatures induce microstructural modifications in biochar, including decreased porosity and increased crystallinity of calcium phosphate phases, further modulating phosphorus release kinetics.

Table 2 provides a comprehensive summary of the fitting outcomes derived from phosphorus release data obtained from fish scale substrates and their corresponding biochars. Three principal empirical models were employed in this analysis: Higuchi model, Korsmeyer–Peppas model, and Peppas–Sahlin model. These models serve to elucidate the phosphorus liberation mechanism by approximating the kinetics of nutrient release from these biocomposite materials. Following the acquisition of both instantaneous release rates and cumulative release profiles, the experimental data were integrated into the DDSolver (1.0) computational framework. This advanced add-in for Excel facilitates the evaluation of release kinetics by employing three critical statistical metrics: the Akaike Information Criterion (AIC), the correlation coefficient (r^2), and the Model Selection Criterion (MSC). The optimal kinetic model is identified by maximizing r^2 and MSC values while concurrently minimizing the AIC.

In the present study, the Higuchi model did not exhibit an adequate fit to the experimental data, presumably due to its oversimplified assumptions relative to the complex release behavior observed. Conversely, the Korsmeyer–Peppas and Peppas–Sahlin models provided superior fits across nearly all samples, as evidenced by higher r^2 values and favorable MSC scores coupled with lower AIC values. This observation suggests that these models are more adept at capturing the multifaceted release dynamics inherent to the system under investigation. From the model fitting procedure, key kinetic parameters were extracted, including the Korsmeyer–Peppas rate constant (K_{KP}) and the transport exponent (n). The data reveal that the fish scale material exhibits a more rapid phosphorus release (K_{KP} = 22.65) compared to the biochars, for which K_{KP} values ranged from 10.92 to 20.03. This discrepancy is attributed to the intrinsic properties of the fish scale, a natural biocomposite, that demonstrates significant swelling behavior in aqueous media, whereas the biochars display a nonporous morphology, resulting in a more constrained diffusion process for phosphorus. Furthermore, transport exponent (n) values ranging between 0.18 and 0.33 indicate that the release mechanism is predominantly governed by Fickian diffusion, underscoring the important key of diffusional transport in these systems.

Additional microstructural characterization, including SEM and EDS, corroborated the kinetic findings by revealing distinct morphological differences between the raw fish scale and the derived biochars (Figure 1). These observations suggest that the reduction in porosity and the evolution of the carbonaceous network induced by high-temperature pyrolysis significantly modulate the diffusion pathways and, consequently, the phosphorus release profiles.

To elucidate the relative contributions of these processes in the phosphorus release system, the Peppas–Sahlin equation was applied, and the derived parameters are summarized in Table 2. In the framework of the Peppas–Sahlin model, the exponent m quantitatively represents the Fickian diffusion mechanism, whereas K_1 and K_2 serve as the rate constants for diffusional transport and matrix erosion, respectively. The analysis indicates that the diffusion-controlled mechanism, as characterized by a higher K_1 value, is predominantly responsible for the release kinetics, whereas the substantially lower K_2 suggests that erosion is a minor contributor under the experimental conditions. Recognizing that the individual values of K_1 and K_2 do not fully capture the complex interplay between Fickian diffusion and erosion, the ratio of erosion to diffusion contributions (R/F) was computed for each sample and plotted against the cumulative phosphorus release from both the fish scale and the pyrolyzed biochars (Figure 7).

TABLE 2 | Parameters of the examined models for P release kinetics.

Model	Parameters	Samples				
			Biochars			
		Fish scales	300°C	400°C	500°C	600°C
Higuchi	K_H ($h^{-0.5}$)	6.8	5.5	5.03	5.5	5.6
	r^2	−0.1	0.81	0.22	−0.46	−0.04
	MSC	−0.31	1.46	0.05	−0.58	−0.24
	AIC	74.79	59.8	67.9	72.9	71.5
Korsmeyer–Peppas	K_{KP} (h^{-n})	22.65	10.92	14.99	20.03	18.29
	n	0.21	0.33	0.23	0.18	0.21
	r^2	0.92	0.94	0.78	0.71	0.76
	MSC	2.12	2.38	1.10	0,83	1.01
	AIC	50.4	50.6	57.4	58.9	58.9
Peppas–Sahlin	K_1 (h^{-m})	17.39	9.25	11.70	15.12	14.05
	K_2 (h^{-2m})	5.63	2.25	3.49	5.00	4.42
	m	0.15	0.25	0.18	0.14	0.16
	r^2	0.93	0.95	0.79	0.72	0.77
	MSC	2.00	2.32	0.96	0.67	0.86
	AIC	51.6	51.2	58.8	60.5	60.5

Note: K_H: Higuchi rate constant; K_{KP}: Korsmeyer–Peppas rate constant; n: Korsmeyer–Peppas transport exponent; K_1: Peppas–Sahlin diffusion rate constant; K_2: Peppas–Sahlin relaxation rate constant; m: Fickian diffusion exponent; r^2: coefficient of correlation.
Abbreviations: AIC, Akaike Information Criterion; MSC, model selection criterion.

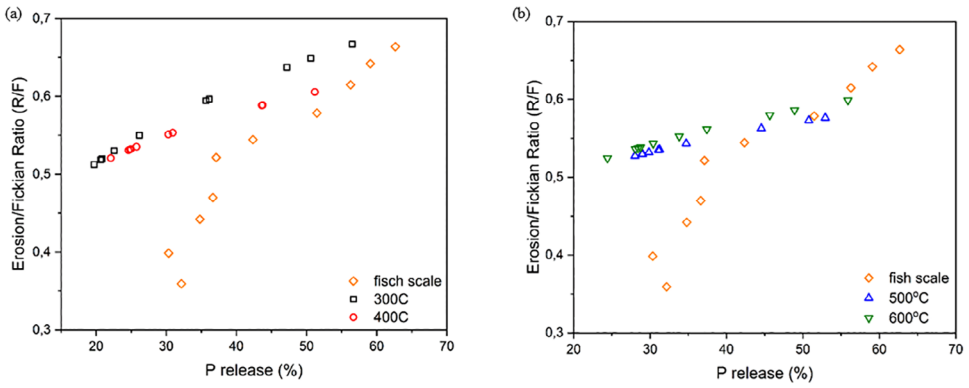

FIGURE 7 | Relaxation (R)/Fickian (F) contribution ratio with the fraction of phosphorus release for biochar pyrolyzed at 300–400°C (A) and 500–600°C (B).

An R/F ratio below unity confirms that, initially, phosphorus liberation is governed primarily by diffusion. However, as time progresses, an increase in the R/F ratio implies that diffusion is approaching equilibrium and that a secondary erosion-dominated mechanism may gradually assume a more significant role in controlling the overall release behavior. These findings underscore the critical interplay between diffusion kinetics and matrix stability in determining nutrient release profiles, thereby providing valuable insights for optimizing controlled-release systems in advanced material applications.

2.6 | Elemental Analysis

Table 3 shows the results of the elemental analysis of the scales and biochars. Regarding carbon composition, the scales presented themselves as the most carbonaceous material (24.75% ± 0.43%). However, with the increase in pyrolysis temperature, the carbon content in the biochars decreased. Although the literature on the pyrolysis of tilapia scales and their elemental composition is still scarce, there are reports of the chemical analysis of biochar from bovine bone meal. The

TABLE 3 | Elemental analysis of materials.

	C (%)	H (%)	N (%)	O (%)	H/C	O/C	C/N
Fish scale	24.75 ± 0.43a	4.47 ± 0.01a	8.82 ± 0.20a	61.96 ± 0.62d	0.02 ± 0.0003a	3.34 ± 0.09c	2.41 ± 0.01c
300°C	13.20 ± 0.55b	2.07 ± 0.01b	4.45 ± 0.26b	80.27 ± 0.81c	0.01 ± 0.0006a	8.11 ± 0.42bc	2.54 ± 0.04bc
400°C	9.56 ± 0.14c	1.36 ± 0.01c	2.97 ± 0.07c	86.11 ± 0.21b	0.012 ± 0.0002ab	12.00 ± 0.21ab	2.76 ± 0.02bc
500°C	6.47 ± 1.01d	0.91 ± 0.01d	1.87 ± 0.16d	90.74 ± 1.19a	0.012 ± 0.0018ab	18.94 ± 3.22a	2.95 ± 0.21b
600°C	8.17 ± 0.2cd	0.82 ± 0.01e	1.82 ± 0.02d	89.18 ± 0.28ab	0.0085 ± 0.0002b	14.54 ± 0.49ab	3.85 ± 0.06a

Note: Results followed by different letters indicate a significant difference ($p > 0.05$) by ANOVA followed by.

authors state that lower pyrolysis temperatures allow a greater amount of organic matter to be carbonized. This fact results in a higher concentration of carbon in samples produced at lower temperatures [22].

As with carbon content, chemical analyses of hydrogen and nitrogen showed higher levels in the scale sample. Consistently, increasing the pyrolysis temperature promotes a reduction in the hydrogen content and other volatile elements in biochars. Because higher thermal conditions intensify the devolatilization and removal of labile functional groups bearing H during carbonization, this results in a more stable and recalcitrant carbon structure [23]. Studies involving biochars produced from animal bones have reported similar behavior. Lower pyrolysis temperatures favor the retention of organic matter and, consequently, higher levels of volatile elements in the carbonized materials [24].

The H/C ratio was significantly lower than the O/C and C/N ratios, indicating that high temperatures altered the structure of the materials, with a significant loss of hydrogen [25]. These results indicate that the chemical composition of these materials is influenced by the pyrolysis temperature.

2.7 | Agronomic Performance

An extensive agronomic evaluation was conducted under controlled greenhouse conditions to assess the impact of fish scale–derived biochars, produced via pyrolysis at 300°C, 400°C, 500°C, and 600°C, on the growth performance of *Triticum aestivum* cultivated in Dystrophic Red Latosol. A commercial phosphate fertilizer served as the control treatment. The agronomic assessments investigated were shoot length (Figure 8A), spike length (Figure 8C), and grain number per pot (Figure 8B).

The results demonstrated that samples of biochar significantly enhanced plant growth relative to the commercial fertilizer. In particular, the biochar produced at 600°C exhibited the most pronounced effect, with shoot length, spike length, and grain number per pot increasing by 25.1%, 18.2%, and 24.2%, respectively, compared to the control. This improvement is attributed to the increased bioavailability of phosphorus, a critical element for photosynthetic efficiency, metabolic activity, and root system development in seedlings. Enhanced nutrient accessibility is linked to the optimized microstructure and surface chemistry of biochars pyrolyzed at high temperature, which facilitate controlled phosphorus release. Studies highlight similar agronomic improvements reported when biochar-based fertilizers can partially replace conventional chemical fertilizers. Replacing these fertilizers with organic fertilizers is a significant agricultural practice that can increase crop productivity and influence soil activity. The increased crop performance and efficiency is attributed to greater phosphorus availability, consequently a controlled release of nutrients, and favorable interactions between biochar and soil, promoting greater efficiency in nutrient absorption by the soil [26].

Table 4 illustrates how biochar pyrolysis temperature modulates soil fertility parameters in wheat-cultivated Oxisol compared with a commercial P fertilizer and pristine soil.

Incorporation of fish scale biochars elevated soil pH in all treatments relative to the acidic control (pH 5.7). Lower temperature chars (300–400°C) produced modest liming effects, increasing pH to ≈6.1–6.3, whereas high-temperature biochars (500–600°C) induced more pronounced alkalinization (pH 6.4). In contrast, commercial P fertilizer left soil pH essentially unchanged (≈5.9). The progressive rise in pH_{pcz} of biochars with temperature (Table 1) underpins this trend, as more refractory mineral oxides form at higher pyrolysis regimes.

Resin-extractable P in biochar-amended soils showed a temperature-dependent bell-shaped profile. The 300–500°C biochar modestly enhanced P availability over pristine soil; maximal gains occurred with 600°C biochars reflecting optimal exposure of labile phosphate groups yielding available P comparable to or exceeding commercial fertilizer.

Mehlich-1 K levels and mono-calcium phosphate extractable sulfur decreased similarly across all biochar treatments, irrespective of pyrolysis temperature, due to inherent K and S adsorption to biochar. In fact, the commercial fertilizer boosted soil K and S due to the presence of these nutrients in its composition.

3 | Conclusion

The material characterization results added to agronomic performance revealed that escalating pyrolysis temperatures induced extensive carbonization and the formation of graphitic-like domains, thereby decreasing porosity. Zero charge potential measurements and in vitro release assays further verified that the 600°C biochar possessed superior nutrient retention

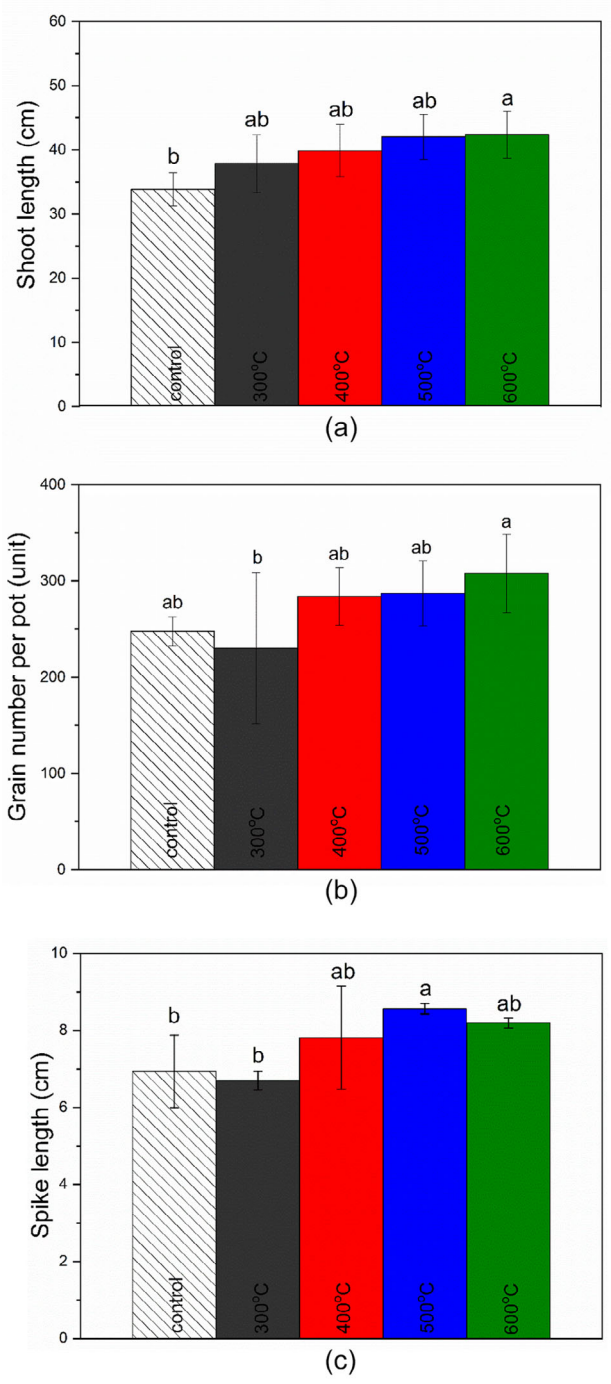

FIGURE 8 | Impact of fertilization with commercial phosphorus fertilizer and four biochar types derived from fish scales on wheat growth characteristics a Dystrophic Red Oxisol. Lowercase letters were used to compare the means of each parameter evaluated between treatments. Shoot length (A) and grain number per pot (B) were obtained by ANOVA followed by the test using Tukey's test ($p < 0.05$). Spike length (C) was compared by Kruskal–Wallis test followed by Dunn's posttest ($p < 0.05$).

and release properties. The integration of these physicochemical insights with agronomic performance data elucidates the structure–property–function relationships underpinning phosphorus diffusion and uptake. Analyzing all the results together, these findings underscore the potential of thermochemically engineered biochars as advanced, sustainable nutrient delivery systems in precision agriculture, aligning with prior studies that demonstrate their efficacy in promoting crop yield and growth.

4 | Experimental Section

4.1 | Materials

Fish scale (*Oreochromis niloticus*) was obtained from Riviera SeaFood, Perdizes, Minas Gerais, Brazil. Hydrochloric acid (36%) and sodium hydroxide (purity ≥ 99%) were supplied by Synth (Diadema, SP, Brazil). Citric acid (purity ≥ 99%), hydrogen peroxide (30% V/V), and nitric acid (65%) were supplied by Êxodo Científica from Brazil. Potassium nitrate (purity ≥ 99%), magnesium sulfate (heptahydrate, $MgSO_4 \cdot 7H_2O$) (purity ≥ 98%), ammonium sulfate (purity ≥ 99%), ammonium nitrate (purity ≥ 99.8%), boric acid (purity ≥ 99.5%), manganese chloride (tetrahydrate, $MnCl_2 \cdot 4H_2O$) (purity ≥ 98%), sodium molybdate (dihydrate, $Na_2MoO_4 \cdot 2H_2O$) (purity ≥ 98%), zinc sulfate (heptahydrate, $ZnSO_4 \cdot 7H_2O$) (purity ≥ 99%), and iron(III) chloride ($FeCl_3$) (purity ≥ 98%) were supplied by Dinâmica Química Contemporânea Ltda (Indaiatuba, SP, Brazil). Triple super phosphate 46% (Yara Brasil Fertilizantes SA). All the chemicals used in this work were of analytical grade and utilized as received without further purification. Deionized water was used in all the experiments.

4.2 | Production and Characterization of Fish Scale Biochar

First, fish scale was dried at 80°C for 48 h and milled in a knife mill (Lucadema—model Luca 226/2). The fish scale samples were then pyrolyzed at four temperatures (300°C, 400°C, 500°C, and 600°C) for 1 h under inert atmosphere using 10°C min^{-1}. After pyrolysis, the charred samples were left to slowly cool down to room temperature. The pH determination of biochar was performed following Rajkovich et al. [28]. Approximately 1.0 g of biochar was mixed with 20 mL of deionized water (ratio 1:20 m v^{-1}). The suspension was stirred for 1.5 h, and then the pH was recorded with a previously calibrated pH electrode [28]. At the end of each cycle, the yield and ash content of the biochars were calculated using Equations (1) and (2), respectively. The ash content was obtained by burning the materials at the same temperatures as the pyrolysis [29]:

$$\text{Biochar yield } (\%) = \left(\frac{\text{mass of residue}}{\text{mass of milled fish scale}} \right) \times 100 \quad (1)$$

$$\text{Ash content } (\%) = \left(\frac{\text{mass of residue}}{\text{mass of milled fish scale}} \right) \times 100 \quad (2)$$

The morphology and microstructure of different fish scale biochar were characterized using SEM (JEOL JSM-6701F, Japan) [30]. Spectroscopic analysis using a Bruker FT-IR spectrometer (model VERTEX 70v) with the Attenuated Total Reflectance (ATR) accessory was performed on the samples in the spectral range of 4000–400 cm^{-1}, with a resolution of 4 cm^{-1} and a scan number of 64 [31]. With the aim of evaluating the pyrolysis conditions, TGA was carried out from room temperature to different temperatures (300°C, 400°C, 500°C, and 600°C) at 10°C min^{-1}

TABLE 4 | Impact of fertilization with commercial phosphorus fertilizer and four biochar types derived from fish scales in the physical–chemical properties of Oxisols Dystrophic Red Latosol before (pristine soil) and after wheat cultivation.

	pH	P	K	S
		mg dm^{-3}		cmol dm^{-3}
Pristine soil	5.7	17.3	186.1	59.8
Control (commercial fertilizer)	5.95 ± 0.12b	37.3 ± 2.8b	205.2 ± 25.2a	102.8 ± 12.8a
300°C	6.32 ± 0.09ab	45.6 ± 8.2b	166.7 ± 18.6ab	12.4 ± 9.3b
400°C	6.12 ± 0.33ab	38.3 ± 5.4b	150.7 ± 18.8b	10.7 ± 4.6b
500°C	6.37 ± 0.12a	34.3 ± 7.4b	153.3 ± 8.7b	21.6 ± 4.6b
600°C	6.42 ± 0.09a	66.2 ± 11.6a	160.1 ± 13.5b	19.4 ± 4.2b

Note: Values are expressed as mean ± standard deviation. Different lowercase letters indicate significant differences between treatments ($p < 0.05$) by one-way ANOVA followed by Tukey's test. pH measured in a soil-water ratio of 1:2.5. P-available phosphorus determined by the resin soil test; K-availability determined by the Mehlich-1 soil test; S determined by extraction with monocalcium phosphate in acetic acid [27].

under an N_2 atmosphere (50 mL min^{-1}) for 1 h employing the thermogravimetric analyzer (DTG-60AH, Shimadzu). After 1 h kept at the temperature, the samples were left to slowly cool down to room temperature. Furthermore, TG experiments were performed under nitrogen atmosphere, at a flow rate of 50 mL min^{-1}. Samples were scanned from room temperature to 800°C at a scanning rate of 10°C min^{-1} using alumina crucibles [32]. The pH at PZC was determined according to the method reported by Mukherjee et al. [33]. Specifically, biochar was added into de-ionized water, and the pH was adjusted to between 3.0 and 12 using diluted NaOH or HCl. Then the solutions were agitated at room temperature for 24 h using shaker incubator (model Q816M22, QUIMIS) to allow them to reach their equilibrium point. The equilibrium pH was measured, the pH change was recorded, and the potential titration curves (pH–ΔpH) were obtained. The PH_{pcz} was the pH that corresponded to ΔpH = 0.

Characterization for total P contents in all samples, following the dry ashing procedure [34], and total elements were determined using ICP-OES Spectro Blue, Spectro Analytical Instruments, Germany).

Biochar samples were analyzed for plant-available phosphorus using extractions with 2% citric acid at a 1:100 (w/v) ratio. The samples were shaken with the extractants for 30 min and filtered through qualitative filter paper. After extraction, the solution was filtered and subsequently analyzed by ICP-OES to quantify the concentration of available phosphorus [35].

Phosphorus in vitro release from the biochars was performed according to the methodology described by Leite et al. [36], in orbital shakers (QUIMIS, model Q816M22) at 35°C and 100 rpm for a total 5-day (120 h) period, in triplicate. Briefly, falcon tubes containing 15 mL 2% citric acid solution and 50 mg samples were incubated for predetermined times (2, 4, 8, 12, 24, 32, 48, 72, 96, and 120 h), and the resulting solution was filtered and analyzed by ICP-OES to obtain the amount of phosphorus released.

The release behavior of the fish scale biochar was evaluated with the help of the Higuchi [37], Korsmeyer–Peppas [38], and Peppas–Sahlin [39]. The first 60% of the release data was analyzed by these models that are described by the following equations, respectively:

$$\frac{M_t}{M_o} = K_H\, t^{1/2} \tag{3}$$

$$\frac{M_t}{M_o} = K_{KP}\, t^{n} \tag{4}$$

$$\frac{M_t}{M_o} = K_1\, t^{m} + K_2 t^{2m} \tag{5}$$

where $\frac{M_t}{M_o}$ is the fractional release at time t (h), K_H is the Higuchi release velocity constant, K_{KP} is the Korsmeyer–Peppas release velocity constant, n is the release exponent that is an indicative of the release mechanism, K_1 and K_2 are kinetic constants for phosphorus release, and m is the diffusional exponent.

The elemental composition of the samples was determined using a CHN elemental analyzer (PerkinElmer EA 2400). Approximately 10 mg of each sample was used for the determination of carbon, hydrogen, and nitrogen contents. The oxygen content was calculated by difference, subtracting the percentages of C, H, and N from the total biochar composition (100%). Molar ratios (H/C, O/C, and C/N) were also calculated.

4.3 | Agronomic Performance of Biochar

Agronomic performance of biochar was evaluated in a controlled greenhouse environment to evaluate the growth of wheat (*T. aestivum*) using surface soil samples (0–20 cm depth) of typical Dystrophic Red Latosol. The soil samples were air-dried, ground, and passed through a 2 mm sieve to obtain air-dried fine earth (ADFE). Soil acidity was neutralized by applying calcium carbonate ($CaCO_3$) and magnesium carbonate ($MgCO_3$) in a 4:1 molar ratio to achieve a target pH of 5.5 ± 0.2. This adjustment was performed to mitigate aluminum toxicity (characteristic of acidic soils) and to optimize the availability of essential macro- and micronutrients, thereby creating favorable growth conditions for the crop. Liming was specifically implemented to enhance the soil's calcium (Ca) and magnesium (Mg) content and improve wheat development [40]. A randomized complete block design

(RCBD) with a 5 × 4 factorial arrangement was employed. The treatments included four biochar types derived from fish scales at various pyrolysis temperatures and a treatment with commercial phosphorus fertilizer treatment. Regardless of the phosphorus source, 200 mg P kg^{-1} soil was applied to the Oxisols [41]. The biochar treatments aimed to assess their potential to improve soil fertility, enhance plant performance, and release phosphorus over time, as analyzed through a kinetic study. Following liming, 5 kg of soil was placed in each pot, fertilized, and sown with five wheat seeds per pot. A nutrient fertilization scheme was adopted, supplying, 100, 200, 50, 40, 0.8, 3.5, 0.1, 5, and 3 mg kg^{-1} of nitrogen (N), potassium (K), sulfur (S), boron (B), manganese (Mn), molybdenum (Mo), zinc (Zn), and iron (Fe), respectively. Fertilizers used included, KNO_3, $MgSO_4 \cdot 7H_2O$, $(NH_4)_2SO_4$, NH_4NO_3, H_3BO_3, $CuSO_4 \cdot 5H_2O$, $MnCl_2 \cdot 4H_2O$, $Na_2MoO_4 \cdot 2H_2O$, $ZnSO_4 \cdot 7H_2O$ and $FeCl_3$ [41]. Seven days after wheat seed germination, some wheat plants were removed, leaving only two wheat plants per pot to carry out the experiment. Irrigation maintained soil moisture at ∼70% of its maximum water-holding capacity. The experiment lasted 96 days, with daily adjustments to water levels. At 96 days post-sowing, 50 g of soil was collected from each experimental unit, dried, and sieved (2 mm). The residual nutrient concentration in the soil was quantified to determine nutrient availability after wheat cultivation [27]. At harvest, 96 days after sowing, wheat plants were separated into shoot, root, and grain fractions. Each component's dry matter (DM) was recorded after drying at 60°C.

4.4 | Statistical Analysis

All data were subjected to the Shapiro–Wilk normality test and Levene's test for homoscedasticity. Parametric data were analyzed by one-way or two-way ANOVA followed by Tukey's test at 5% probability. Nonparametric data were analyzed using the Kruskal–Wallis test followed by Dunn's posttest at 5% probability. SigmaPlot and InfoStat software were used for data analysis.

Author Contributions

Guilherme S. Vitor: writing – original draft, writing – review and editing, investigation, data curation, formal analysis, investigation. **Andressa M. Paiva**: data curation, formal analysis, investigation, writing – review and editing. **Túlio P. Boaventura**: conceptualization, data curation, formal analysis, visualization, writing – review and editing. **Leônidas C. Azevedo Melo**: conceptualization, formal analysis, resources. **Juliano E. Oliveira**: conceptualization, writing – original draft, project administration, funding acquisition.

Acknowledgments

The authors thank FINEP/MCT, CNPq (305532/2024-3, 403724/2023-6, 405802/2022-6, 409365/2024-6, 406925/2022-4), CAPES, and FAPEMIG (APQ-05593-24, APQ-00906-17, BPD-00406-22) for their financial support.

The Article Processing Charge for the publication of this research was funded by the Coordenação de Aperfeiçoamento de Pessoal de Nível Superior - Brasil (CAPES) (ROR identifier: 00x0ma614).

Funding

This study was supported by FINEP/MCT, CNPq (305532/2024-3, 403724/2023-6, 405802/2022-6, 409365/2024-6, 406925/2022-4), CAPES and FAPEMIG (APQ-05593-24, APQ-01713-25, APQ-00906-17, BPD-00406-22).

Conflicts of Interest

The authors declare no conflicts of interest.

Data Availability Statement

The data that support the findings of this study are available from the corresponding author upon reasonable request.

References

1. U. Sittitut, J. Jettanasen, S. Supothina, and R. Rattanakam, "Dissolution Performance of Carbon/Hydroxyapatite Nanocomposite Prepared From Fish Scales," *Inorganics* 10 (2022): 242.

2. N. Rambhatla, T. F. Panicker, R. K. Mishra, S. K. Manjeshwar, and A. Sharma, "Biomass Pyrolysis for Biochar Production: Study of Kinetics Parameters and Effect of Temperature on Biochar Yield and Its Physicochemical Properties," *Results in Engineering* 25 (2025): 103679, https://doi.org/10.1016/j.rineng.2024.103679.

3. L. Zhang, L. Chang, H. Liu, M. de Jesús Puy Alquiza, and Y. Li, "Biochar Application to Soils Can Regulate Soil Phosphorus Availability: A Review," *Biochar* 7 (2025): 13, https://doi.org/10.1007/s42773-024-00415-1.

4. A. Waheed, H. Xu, X. Qiao, et al., "Biochar in Sustainable Agriculture and Climate Mitigation: Mechanisms, Challenges, and Applications in the Circular Bioeconomy," *Biomass and Bioenergy* 193 (2025): 107531, https://doi.org/10.1016/j.biombioe.2024.107531.

5. A. Fakhar, S. J. C. Galgo, R. C. Canatoy, et al., "Advancing Modified Biochar for Sustainable Agriculture: A Comprehensive Review on Characterization, Analysis, and Soil Performance," *Biochar* 7 (2025): 8, https://doi.org/10.1007/s42773-024-00397-0.

6. Z. Xu, R. Zhou, and G. Xu, "Global Analysis on Potential Effects of Biochar on Crop Yields and Soil Quality," *Soil Ecology Letters* 7 (2025): 240267, https://doi.org/10.1007/s42832-024-0267-x.

7. S. P. Sohi, E. Krull, E. Lopez-Capel, and R. Bol, *Advances in Agronomy* (Academic Press, 2010).

8. Y. Yang, G. Li, X. Yue, et al., "Advances in Biochar Composites for Environmental Sustainability," *Advanced Composites and Hybrid Materials* 8 (2024): 74, https://doi.org/10.1007/s42114-024-01181-1.

9. W. A. Srisathan, W. Worrakittikul, K. Rattanapon, T. Hongto, A. Phrommasakha Na Sakhonnakon, and P. Naruetharadhol, "Digitalisation to Zero-Waste: The Interplay of Open Eco-Innovation and the Circular Economy in Agricultural Enterprises," *International Journal of Sustainable Engineering* 18 (2025): 1–21, https://doi.org/10.1080/19397038.2024.2446771.

10. A. B. Dauda, A. Ajadi, A. S. Tola-Fabunmi, and A. O. Akinwole, "Waste Production in Aquaculture: Sources, Components and Managements in Different Culture Systems," *Aquaculture and Fisheries* 4 (2019): 81–88, https://doi.org/10.1016/j.aaf.2018.10.002.

11. S. R. Golroudbary, M. El Wali, and A. Kraslawski, "Environmental Sustainability of Phosphorus Recycling From Wastewater, Manure and Solid Wastes," *Science of the Total Environment* 672 (2019): 515–524, https://doi.org/10.1016/j.scitotenv.2019.03.439.

12. R. A. Cabeza, B. Steingrobe, and N. Claassen, "Phosphorus Fractionation in Soils Fertilized With Recycled Phosphorus Products," *Journal of Soil Science and Plant Nutrition* 19 (2019): 611–619, https://doi.org/10.1007/s42729-019-00061-8.

13. T. Safronova, V. Vorobyov, N. Kildeeva, et al., "Inorganic Powders Prepared From Fish Scales," *Ceramics* 5 (2022): 484–498.

14. P. S. Bindraban, C. O. Dimkpa, and R. Pandey, "Exploring Phosphorus Fertilizers and Fertilization Strategies for Improved Human and Environmental Health," *Biology and Fertility of Soils* 56 (2020): 299–317, https://doi.org/10.1007/s00374-019-01430-2.

15. D. Xia, Y. Liu, X. Cheng, P. Gu, Q. Chen, and Z. Zhang, "Temperature-Tuned Fish-Scale Biochar With Two-Dimensional Homogeneous Porous Structure: A Promising Uranium Extractant," *Applied Surface Science* 591 (2022): 153136, https://doi.org/10.1016/j.apsusc.2022.153136.

16. A. N. Módenes, G. Bazarin, C. E. Borba, et al., "Tetracycline Adsorption by Tilapia Fish Bone-Based Biochar: Mass Transfer Assessment and Fixed-Bed Data Prediction by Hybrid Statistical-Phenomenological Modeling," *Journal of Cleaner Production* 279 (2021): 123775, https://doi.org/10.1016/j.jclepro.2020.123775.

17. H. Zhou, J. Guo, H. Liu, J. Wang, and Y. Wang, "Effects of Biochar Pyrolysis Temperature and Application Rate on Saline Soil Quality and Maize Yield," *Agronomy* 14, no. 7 (2024): 1529, https://doi.org/10.3390/agronomy14071529.

18. L. Chen, N. A. Al-Dhabi, W. Ai, et al., "Impact of Low-Temperature Pyrolysis on Ash and Physicochemical Properties of Straw Biochar: Multivariate Analysis and Implications for Agricultural and Environmental Use," *Industrial Crops and Products* 224 (2025): 120431, https://doi.org/10.1016/j.indcrop.2024.120431.

19. C. Piccirillo, "Preparation, Characterisation and Applications of Bone Char, a Food Waste-Derived Sustainable Material: A Review," *Journal of Environmental Management* 339 (2023): 117896, https://doi.org/10.1016/j.jenvman.2023.117896.

20. A. Mlonka-Mędrala, S. Sobek, M. Wądrzyk, et al., "Kinetics Study and Py-GC-MS Analysis of Pyrolysis in Chicken Bone Waste for Sustainable Utilisation in Thermal Conversion," *Journal of Environmental Management* 373 (2025): 123515, https://doi.org/10.1016/j.jenvman.2024.123515.

21. Y. Liang, X. Cao, L. Zhao, X. Xu, and W. Harris, "Phosphorus Release From Dairy Manure, the Manure-Derived Biochar, and Their Amended Soil: Effects of Phosphorus Nature and Soil Property," *Journal of Environmental Quality* 43, no. 4 (2014): 1504–1509.

22. M. Zupančič and N. Č. Korošin, "Physico-Chemical Properties of the Pyrolytic Residue Obtained by Different Treatment Conditions of Meat and Bone Meal," *Acta Chimica Slovenica* 68, no. 1 (2021): 229–238.

23. A. Y. Elnour, A. A. Alghyamah, H. M. Shaikh, et al., "Effect of Pyrolysis Temperature on Biochar Microstructural Evolution, Physicochemical Characteristics, and Its Influence on Biochar/Polypropylene Composites," *Applied Sciences (Switzerland)* 9, no. 6 (2019): 1149, https://doi.org/10.3390/app9061149.

24. I. de Oliveira Paiva, E. G. de Morais, K. Jindo, and C. A. Silva, "Biochar N Content, Pools and Aromaticity as Affected by Feedstock and Pyrolysis Temperature," *Waste and Biomass Valorization* 15, no. 6 (2024): 3599–3619, https://doi.org/10.1007/s12649-023-02415-x.

25. E. Taskin, C. de Castro Bueno, I. Allegretta, R. Terzano, A. H. Rosa, and E. Loffredo, "Multianalytical Characterization of Biochar and Hydrochar Produced From Waste Biomasses for Environmental and Agricultural Applications," *Chemosphere* 233 (2019): 422–430.

26. C. Ding, X. Luo, Y. Wang, et al., "Partial Replacement of Chemical Fertilizer by Biochar-Based Fertilizer Increases Rice Yield and Soil Quality," *Agronomy* 15, no. 12 (2025): 2716, https://doi.org/10.3390/agronomy15122716.

27. P. C. Teixeira, G. K. Donagemma, A. Fontana, and W. G. Teixeira, *Manual de Métodos de Análise de Solo*, 3a ed. (Embrapa Brasil, 2017).

28. S. Rajkovich, A. Enders, K. Hanley, C. Hyland, A. R. Zimmerman, and J. Lehmann, "Corn Growth and Nitrogen Nutrition After Additions of Biochars With Varying Properties to a Temperate Soil," *Biology and Fertility of Soils* 48, no. 3 (2012): 271–284, https://doi.org/10.1007/s00374-011-0624-7.

29. C. Chen, W. Chen, M. Zhou, et al., "Co-ZIF Reinforced Kraft Lignin Biochar as an Efficient Catalyst for Highly Selective Hydrodeoxygenation of Lignin-Derived Chemicals," *Chemical Engineering Journal* 492 (2024): 152353, https://doi.org/10.1016/j.cej.2024.152353.

30. H. Shin, D. Tiwari, and D. Kim, "Phosphate Adsorption/Desorption Kinetics and P Bioavailability of Mg-Biochar From Ground Coffee Waste," *Journal of Water Process Engineering* 37 (2020): 101484, https://doi.org/10.1016/j.jwpe.2020.101484.

31. S. H. Lee, K. H. Lee, S. Lee, et al., "Conversion of N-Doped Biochar From Carotenoid-Extracted *Tetraselmis suecica* and Its Application to Produce Supercapacitors," *Journal of Environmental Sciences* 151 (2025): 410–423, https://doi.org/10.1016/j.jes.2024.03.039.

32. Z. Junjian, S. Yue, Z. Jigang, and P. Jianghong, "Study on Isothermal Pyrolysis Characteristics and Kinetics of Coarse-Grained Coal Gangue," *Solid Fuel Chemistry* 57 (2023): 95–100, https://doi.org/10.3103/S0361521923030060.

33. A. Mukherjee, A. R. Zimmerman, and W. Harris, "Surface Chemistry Variations Among a Series of Laboratory-Produced Biochars," *Geoderma* 163 (2011): 247–255, https://doi.org/10.1016/j.geoderma.2011.04.021.

34. A. Enders and J. Lehmann, "Comparison of Wet-Digestion and Dry-Ashing Methods for Total Elemental Analysis of Biochar," *Communications in Soil Science and Plant Analysis* 43 (2012): 1042–1052, https://doi.org/10.1080/00103624.2012.656167.

35. B. Singh, M. Camps-Arbestain, and J. Lehmann, *Biochar: A Guide to Analytical Methods* (CSIRO Publishing, 2017).

36. A. D. A. Leite, L. C. A. Melo, L. C. C. Hurtarte, et al., "Magnesium-Enriched Poultry Manure Enhances Phosphorus Bioavailability in Biochars," *Chemosphere* 331 (2023): 138759, https://doi.org/10.1016/j.chemosphere.2023.138759.

37. K. Alharbi, A. Ghoneim, A. Ebid, H. El-Hamshary, and M. H. El-Newehy, "Controlled Release of Phosphorous Fertilizer Bound to Carboxymethyl Starch-g-Polyacrylamide and Maintaining a Hydration Level for the Plant," *International Journal of Biological Macromolecules* 116 (2018): 224–231, https://doi.org/10.1016/j.ijbiomac.2018.04.182.

38. N. Lakshani, H. S. Wijerathne, C. Sandaruwan, N. Kottegoda, and V. Karunarathne, "Release Kinetic Models and Release Mechanisms of Controlled-Release and Slow-Release Fertilizers," *ACS Agricultural Science & Technology* 3 (2023): 939–956, https://doi.org/10.1021/acsagscitech.3c00152.

39. C. G. Chiaregato, C. F. Souza, and R. Faez, "The Fertilizer Release Into Water and Soil as the Biodegradation Process in the Sustainable Material Enhancing the Fertilizer Efficiency," *Environmental Technology & Innovation* 22 (2021): 101417, https://doi.org/10.1016/j.eti.2021.101417.

40. L. Chisté, C. A. Silva, F. H. S. Rabêlo, K. Jindo, and L. C. A. Melo, "Evaluating Copper-Doped Biochar Composites for Improving Wheat Nutrition and Growth in Oxisols," *Agronomy* 15 (2025): 144, https://doi.org/10.3390/agronomy15010144.

41. A. D. A. Leite, I. A. D. D. Resende, B. C. Lago, et al., "Increasing the Fertilizer Efficiency of Potassium Silicate by Co-Pyrolysis and Chemical Activation," *Journal of Soil Science and Plant Nutrition* 24 (2024): 2249–2262, https://doi.org/10.1007/s42729-024-01704-1.